# Investigation of the $_{74}$W $L$ emission spectra and satellites

Aurel-Mihai Vlaicu,* Tatsunori Tochio, Takashi Ishizuka, Daisuke Ohsawa, Yoshiaki Ito, and Takeshi Mukoyama
*Institute for Chemical Research, Kyoto University, Uji, Kyoto 611, Japan*

Atsusi Nisawa and Takasi Shoji
*X-ray Research Institute, Rigaku Corporation, Ibaraki, Osaka 567, Japan*

Sinzo Yoshikado
*Department of Electronics, Doshisha University, Tsuduki-gun, Kyoto 610-03, Japan*
(Received 6 March 1998)

The $L\alpha$ and $L\beta$ spectra of tungsten were measured using a high-resolution single-crystal x-ray spectrometer. The observed spectra were fitted into Lorentzians. The fit residuals of the $L\alpha$ and $L\beta$ spectra indicate the presence of satellites in the vicinity of each spectrum, which are originated from Coster-Kronig transitions. Linewidths, energies, and intensities were estimated for each diagram line and compared with previous data. The $L\beta_2$ satellite line observed by Salgueiro *et al.* [J. Phys. (Paris), Colloq **48**, C9-609 (1987)] was confirmed on the high energy side of the $L\beta_2$ line. The origin of this satellite is discussed experimentally and theoretically. [S1050-2947(98)02011-3]

PACS number(s): 32.30.Rj, 32.80.Hd

## I. INTRODUCTION

It is generally difficult to analyze $L$ x-ray emission spectra induced by excitation with electrons and high-energy photons, where all the three $L$ subshells can be ionized and the subsequent redistribution of initial vacancies occurs by Coster-Kronig transitions. The existence of two or more holes in atomic inner shells gives rise to satellite lines with energies that are shifted from the diagram lines. The study of $L$ x-ray satellites in high-$Z$ elements has not been performed by many workers. For the last 20 years, there are only a few papers on this subject for tungsten $_{74}$W [1–3]. The $L$ x-ray satellite lines usually appear in a slightly higher-energy side than their diagram line. The satellites corresponding to $M$ spectator holes lead to lines that can be resolved well from the parent lines, whereas those corresponding to $N$ spectator holes almost coincide with the diagram lines.

The widths of some $L$ x-ray lines of W were measured as part of a program for compiling the $L$-series linewidths in heavy elements [4–6]. They suggested that the disagreement between theory and experiment was due to the large theoretical values of $M$ and $N$ subshell partial widths calculated by McGuire nonrelativistically [7–9]. However, the existence of hidden satellites was not considered in their analysis of experimental data. It is interesting to measure the $L$ x-ray linewidth of W with higher resolution taking into account the hidden satellite lines.

On the other hand, Salgueiro *et al.* [3] observed the satellite line in the high region of $L\beta_2$ spectrum of W. They concluded that this line was due to Coster-Kronig transitions $L_1$-$L_3M_5$, which were energetically forbidden for $50 \leqslant Z \leqslant 74$ and were allowed for $Z \geqslant 75$ according to the work of Chen *et al.* [10], based on the experimental results of the ratio of the ionization cross sections of subshells $L_1$ and $L_3$ $(\sigma 1/\sigma 3)$, which increase abruptly at 13 keV incident electron energy and become constant for energies above 20 keV.

In the present study, we investigated the linewidth, energies, and intensities including satellites of W $L\alpha$ and $\beta$ emission lines generated by electron bombardment using a single-crystal high-resolution x-ray spectrometer for the evaluation on the correctness of the theoretical calculation of different types of transition rates. In addition, the intensity measurement is executed using various incident electron energies for the satellite in the higher-energy region of $L\beta_{2,15}$ in order to elucidate the mechanism of the origin of this satellite.

## II. EXPERIMENT

The tungsten $L$ spectral lines were excited by electron bombardment in a rotating anode at the tube voltage of 49 kV and the current of 150–180 mA. The spectral measurements were carried out with a single-crystal spectrometer with symmetrical Si(440), Si(444), and Ge(444) perfect crystals in which x-ray topography showed no dislocation. A double slit collimator of 100-mm length and the vertical width of 10 or 20 $\mu$m was used for the measurement. Measuring time was registered so as to obtain at least 10 000 counts per each point in the region of interest. No smoothing was applied to the raw data. For the diagram line the values by Bearden [11] and Sandström [12] were used as reference. The dependence of the detection efficiency on the energy in the $Ar_{0.9}(CH_4)_{0.1}$ flow proportional counter (FPC) was taken into account when calculating the relative intensity of each diagram line.

It is very important for spectral intensity measurement with a x-ray spectrometer to extract the ''true'' emission line from the measured and instrumentally distorted profile. The influence of the instrumental function was minimized already in the measurement process itself by an optimal selection of the experimental setup in our experiments, i.e., the influence

*Author to whom correspondence should be addressed. Address correspondence to National Institute for Material Physics, P. O. Box MG-7, 76900 Magurele, Bucharest, Romania.

 

TABLE I. Natural linewidth of W $L$ diagram lines at 49 kV exciting energy: theoretical values are compared with experimental values using multiplet fitting; experimental values by Salem *et al.* [5] are compared with experimental values obtained by single peak fitting. For the Lorentzian profile the values are corrected using Eq. (1). The correction factor ($n$) is given in parentheses.

| Line | Transition | Energy (eV) | Linewidths (eV) | | | | | | | | | |
|---|---|---|---|---|---|---|---|---|---|---|---|---|
| | | Bearden | Theoretical | | | Multiplet fit | | | Salem [5] | Single peak fit | | |
| | | | $\Gamma_i$ | $\Gamma_f$ | $\Gamma_{\text{theor}}$ | Voigt | Lorentz | ($n$) | experimental | Voigt | Lorentz | ($n$) |
| W $L\alpha_1$ | $L_3$-$M_5$ | 8397.6 | 4.812 | 1.795 | 6.607 | 6.8(4) | 6.7(8) | (1.31) | 7.84±0.63 | 7.0(5) | 7.022 | (1.33) |
| W $L\alpha_2$ | $L_3$-$M_4$ | 8335.2 | 4.812 | 1.868 | 6.680 | 6.8(6) | 6.8(6) | (1.42) | 5.27±0.53 | 7.3(1) | 6.(4) | (1.43) |
| W $L\beta_2$ | $L_3$-$N_5$ | 9961.5 | 4.812 | 7.720 | 12.532 | 9.6(5) | 8.9(8) | (1.33) | 9.26±0.93 | 10.9(0) | 10.3(9) | (1.32) |
| W $L\beta_{15}$ | $L_3$-$N_4$ | 9947.8 | 4.812 | 7.89 | 12.702 | 10.2(6) | 9.(2) | (1.1) | | 8.2(2) | 7.(4) | (1.2) |
| W $L\beta_1$ | $L_2$-$M_4$ | 9672.35 | 4.821 | 1.868 | 6.689 | 6.6(7) | 6.4(8) | (1.62) | 7.82±0.63 | 6.9(0) | 6.7(6) | (1.67) |
| W $L\gamma_1$ | $L_2$-$N_4$ | 11 285.9 | 4.821 | 7.89 | 12.711 | 9.7(7) | 9.(8) | (2.13) | 10.20±1.02 | 10.6(5) | 10.(7) | (2.20) |
| W $L\beta_3$ | $L_1$-$M_3$ | 9818.8 | 5.959 | 10.560 | 16.519 | | | | 12.6±1.26 | 12.6(5) | 12.6(2) | (1.72) |
| W $L\beta_4$ | $L_1$-$M_2$ | 9525.2 | 5.959 | 11.90 | 17.859 | | | | 13.20±1.45 | 14.9(0) | 14.3(4) | (1.21) |

of the collimator geometry, the crystal reflection properties (as given by the dynamical theory of x-ray diffraction), and the tube arrangement for the absorption were taken into account.

## III. RESULTS AND DISCUSSION

### A. Spectra analysis and correction factors

In order to extract the natural linewidth ($\Gamma_n$) from the measured spectral linewidth ($\Gamma_0$) one has to correctly evaluate the dispersion of the spectrometer. In our case we considered the contribution to the observed linewidth due to the double slit collimator ($\delta E_{\text{slit}}$), and due to the reflection on the crystal ($\delta E_{\text{crystal}}$), which is usually much smaller than the first one. Therefore, the total observed spectral broadening can be expressed as the sum of the two components.

An attempt to evaluate the natural linewidths was made by using the following empirical formula:

$$\Gamma_{\text{obs}}^n = \Gamma_{\text{nat}}^n + (\delta E_{\text{slit}} + \delta E_{\text{crystal}})^n, \tag{1}$$

where $n$ is the correction factor, with values in the range $1 < n < 2$. This equation is a generalization of the relation for the widths obtained by convoluting two Lorentzian distributions ($n=1$), or two Gaussian distributions ($n=2$). We considered for each line two experimental setups, with different spectral broadening, and fitted the spectra into Lorentzians. The values thus obtained for $\Gamma_{\text{obs}}$, $\delta E_{\text{slit}}$, and $\delta E_{\text{crystal}}$ from the two setups were used as input values for the following system of equations:

$$\Gamma_{\text{obs}(1)}^n = \Gamma_{\text{nat}}^n + (\delta E_{\text{slit}(1)} + \delta E_{\text{crystal}(1)})^n,$$

$$\Gamma_{\text{obs}(2)}^n = \Gamma_{\text{nat}}^n + (\delta E_{\text{slit}(2)} + \delta E_{\text{crystal}(2)})^n. \tag{2}$$

The system of equations was numerically solved by iterative methods and the natural width $\Gamma_{\text{nat}}$, and the correction factor ($n$) were obtained. The main demerit of this method is the underestimation of $\Gamma_{\text{obs}}$ while fitting the spectra using Lorentzian distributions. Hence, the obtained natural linewidths are also underestimated. Second, the convergency of the system of equations (2) is very sensitive to the input values.

In order to avoid this limitation, we analyzed our spectra using Voigt functions also, which can be written in terms of position ($E_0$), amplitude ($A$), Lorentzian width ($w$), and dispersion width ($d$) as follows:

$$V(E,E_0,A,w,d) = V(x,y) = A\frac{K(x,y)}{K(0,y)} \tag{3}$$

where

$$K(x,y) = \frac{y}{\pi}\int \frac{e^{-t^2}}{y^2+(x-t)^2}\,dt \tag{4}$$

represents the convolution of a Lorentzian with a Gaussian. The first parameter, ($x$), represents the energy axis ($E$) in units of dispersion ($d$):

$$x = 2\sqrt{\ln(2)}\ \frac{E-E_0}{d} \tag{5}$$

and the second parameter, ($y$), represents the shape of the Voigt function:

$$y = \sqrt{\ln(2)}\ \frac{w}{d}. \tag{6}$$

Various computational methods for the evaluation of the integral in Eq. (4) can be found elsewhere [13–17]. Details about the Voigt function in this form are given in Sec. VI.

Both methods are affected by the precision of the evaluation of the spectral broadening. Because one cannot determine all instrumental dispersion factors, the spectral broadening tends to be always underevaluated and the obtained natural linewidths tend to be therefore larger than the true linewidths. This happens for both methods. For the correction factor method [see Eq. (2)], the obtained natural linewidths are slightly smaller. This is because the spectra are

fitted with Lorentzian functions instead of Voigt functions. Obtaining close values with both methods shows a good evaluation of the spectral broadening, and one can identify measurements where additional spectral broadening factors are present, for example, due to misalignment, bad focusing, etc. Although we present our result obtained with both methods, we recommend to consider only the results obtained by using the Voigt fitting method.

### B. Diagram lines

Theoretical values of natural width of atomic vacancy states were reported for the *L* shell [18], and the *M* shell [19,20] using the relativistic calculations, and for the *N* shell with nonrelativistic calculations [21,22]. The natural width of an x-ray line originated from a transition from an atomic level (*A*) to a level (*B*) is represented as the sum of the width of the initial and final levels:

$$\Gamma(A-B)=\Gamma(A)+\Gamma(B). \tag{7}$$

The experimental values for the natural width of diagram lines were obtained using the multiplet fitting method by Deutsch *et al.* [23], considering the satellite structure, with the only difference that for the peak shape we used not only the Lorentzian profile but also the Voigt profile for comparison:

$$I_s(E)=\sum_{m=1}^{M} A_m \sum_{l=1}^{L} p_l(E,E_{lm}-s_m,b_{lm},w_m,d_m), \tag{8}$$

where $p(E)$ can be the Lorentzian or the Voigt profile. A linear background is also added to the profile.

In Eq. (8), the indices ($m$) denote the multiplets and the indices ($l$) denote the lines within a given multiplet. Prior to fitting one has to calculate the positions of the diagram and satellite lines ($E_{lm}$) and the relative intensities ($b_{lm}$) of the satellite lines to the diagram lines, which are all fixed parameters in the fitting procedure. Within a multiplet, the amplitude ($A_m$), the energy shift ($s_m$) relative to the calculated position, the width ($w_m$), and the dispersion ($d_m$)—in the case of using the Voigt profile—are common for all lines within the multiplet. These last four parameters are free during the fitting, and are actually the result of the fitting. However, we chose to fix during the fitting also the dispersion parameters to the values calculated for each diagram line using the geometry of the collimator and the dispersion of the crystal.

The values for the energy positions of the satellite lines were taken from the table published by Parente [25]. The theoretical values for linewidths are estimated as the sum of the two levels involved in the transition. In the next section we show the model for calculating the relative intensity of the satellite lines. In addition, for comparison of our results with previous experimental values obtained by Salem [4,5], each diagram line was also fitted into single symmetric Lorentzians. The natural linewidths obtained in our experiment are compared in Table I with the values derived from theoretical calculations and with previous experimental results.

For the transitions involving *L*-shell levels and *M*-shell levels, such as $L\alpha_1$, $L\alpha_2$, $L\beta_1$, $L\beta_3$, and $L\beta_4$, we have a good agreement between the values obtained by multiplet fitting and the theoretical values, which are obtained using the relativistic calculations. On the other hand, for the transitions involving *L*-shell levels and *N*-shell levels, such as $L\beta_2$, $L\beta_{15}$, $L\gamma_1$, the widths obtained from theoretical calculations are all larger with the difference between 2.7 eV and 3.3 eV. This disagreement between theory and experiment for $L_i \rightarrow N_j$ transitions can be attributed to the values for the *N*-shell vacancy states obtained from nonrelativistic calculations. Although Gokhale *et al.* [6] and Salem and Lee [4] also suggested this, they did not consider the satellite structure for each spectrum.

Normally, while considering the satellite structure in the multiplet fitting method, the obtained natural linewidths are smaller compared with those obtained by single Lorentzian fitting. In the case of $L\beta_{15}$, which is very close to $L\beta_2$, we obtained an opposite result due to the overlapping of the two spectra.

The relative intensities derived from the radiative transition probabilities published by Scofield [24] are shown in Table II together with the experimental values obtained by Salem *et al.* and our experimental values obtained both in the case of single Lorentzian fitting and in the case of multiplet fitting. In order to avoid the dependence of the ionization cross section on exciting electron energy $\sigma_{i=1,2,3}(E)$, we have to compare separately the relative intensities of the diagram lines that have a different initial vacancy state.

We can observe again that in the case of $L\beta_{15}$, the relative intensity obtained by using the multiplet fitting method is higher than the value obtained by using single Lorentzian fitting. This explains also why the measured value of the relative intensity of the $L\beta_2$ satellite is higher in the case of multiplet fitting.

The structure left in the residue of fitting by using single Lorentzians may be attributed to the presence of the hidden satellites. However, even after considering the satellite structure by using the multiplet fitting method, there still remains some structure in the residue (see Fig. 1). We encountered this situation for all analyzed spectra, excluding $L\beta_{2,15}$, where after using the multiplet fitting method, the residue was reduced to background level (see Fig. 2). This can be due to the fact that we could not include in the multiplet fitting model the contribution of the *O*-shell and *P*-shell spectator hole and the shake-off processes. Also, the spectra are affected by the dispersion of the spectrometer. If possible, it is generally recommended to deconvolute the spectra prior to analysis or to analyze the spectra using Voigt functions that include the dispersion of the spectrometer.

### C. Satellites from Coster-Kronig transitions

The relative intensities of Coster-Kronig satellite transitions are calculated assuming that the fluorescence yields $\omega_{i,i=1,2,3}$ has the same value for both the case of single vacancy states and multiple vacancy states. In the transitions to the initial vacancy state $L_2$, the relative intensities of the spectator hole satellite lines to the diagram line can be calculated as follows:

TABLE II. Relative intensities of W $L$ emission lines: Theoretical values are compared with experimental values obtained by multiplet fitting; experimental values obtained by Salem *et al.* [5] are compared with the experimental values obtained by single peak fitting. For the Voigt profile we used the area of the Voigt function as given in Eq. (A4). *, for $L\beta_{3,4}$, different experimental settings could not establish the same relative intensity.

| Line | Transition | Relative intensity $I_{rel}$ (%) | | | | | |
|---|---|---|---|---|---|---|---|
| | | Scofield [24] | Multiplet fit | | Salem [5] | Single peak fit | |
| | | theoretical | Voigt | Lorentzian | experimental | Voigt | Lorentzian |
| W $L\alpha_1$ | $L_3$-$M_5$ | 100 | 100 | 100 | 100 | 100 | 100 |
| W $L\alpha_2$ | $L_3$-$M_4$ | 11.34 | 11.2(7) | 11.3(0) | 11.16 | 11.4(1) | 11.4(3) |
| W $L\beta_{2,15}$ | $L_3$-$N_{5,4}$ | 19.64 | 24.2(2) | 24.1(7) | 22.74 | 24.3(2) | 24.5(1) |
| W $L\beta_2$ | $L_3$-$N_5$ | 17.74 | 21.3(5) | 21.4(5) | | 22.6(4) | 22.8(5) |
| W $L\beta_{15}$ | $L_3$-$N_4$ | 1.98 | 2.8(7) | 2.7(2) | | 1.6(8) | 1.6(6) |
| W $L\beta_2$ | $L_3$-$N_5$ | 100 | 100 | 100 | | 100 | 100 |
| W $L\beta_{15}$ | $L_3$-$N_4$ | 11.16 | 13.4(8) | 12.7(0) | | 7.4(0) | 7.2(3) |
| W $L\beta_1$ | $L_2$-$M_4$ | 100 | 100 | 100 | 100 | 100 | 100 |
| W $L\gamma_1$ | $L_2$-$N_4$ | 18.61 | 26.1(0) | 26.8(7) | 18.80 | 26.7(6) | 26.9(8) |
| W $L\beta_3$ | $L_1$-$M_3$ | 100 | | | 100 | * | * |
| W $L\beta_4$ | $L_1$-$M_2$ | 79.88 | | | 67.8 | * | * |

$$I_s(L_2)=(\sigma_1/\sigma_2)f_{1,2}P(L_1L_2X), \tag{9}$$

where $\sigma_i$, $_{i=1,2,3}$, is the ionization cross section by electrons for the $L_i$ subshell; $f_{i,j}$ is the partial Coster-Kronig transition probability from the $L_i$ to the $L_j$ the level; $P(L_iL_jX)$ is the probability of the radiationless transition $L_i \rightarrow L_jX$, for which the double vacancy state $L_jX$ is created, where $X$ is either an $M$ or an $N$ shell. In the transitions to the initial vacancy state $L_3$, there are two possible Coster-Kronig transitions: $L_1 \rightarrow L_3X$ and $L_2 \rightarrow L_3X$. The relative intensities of the spectator hole satellite lines to the diagram line has three terms:

$$\begin{aligned} I_s(L_3)=&(\sigma_1/\sigma_3)f_{1,3}P(L_1L_3X)+(\sigma_2/\sigma_3)f_{2,3}P(L_2L_3X)\\ &+(\sigma_1/\sigma_3)f_{1,2}f_{2,3}\{P(L_1L_2X)[1-P(L_1L_3X)]\\ &+[1-P(L_1L_2X)]P(L_1L_3X)\}. \end{aligned} \tag{10}$$

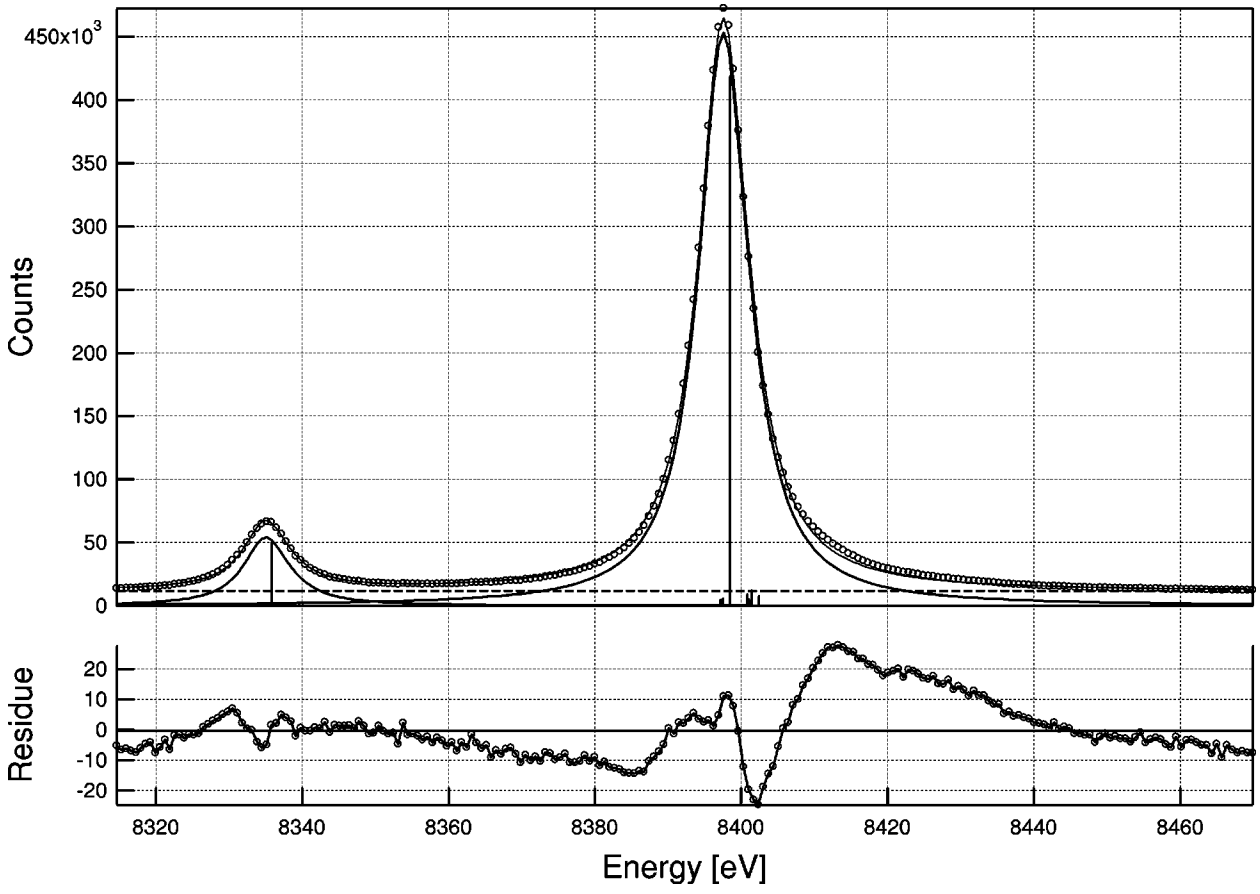


FIG. 1. W $L\alpha_{1,2}$ emission spectra.

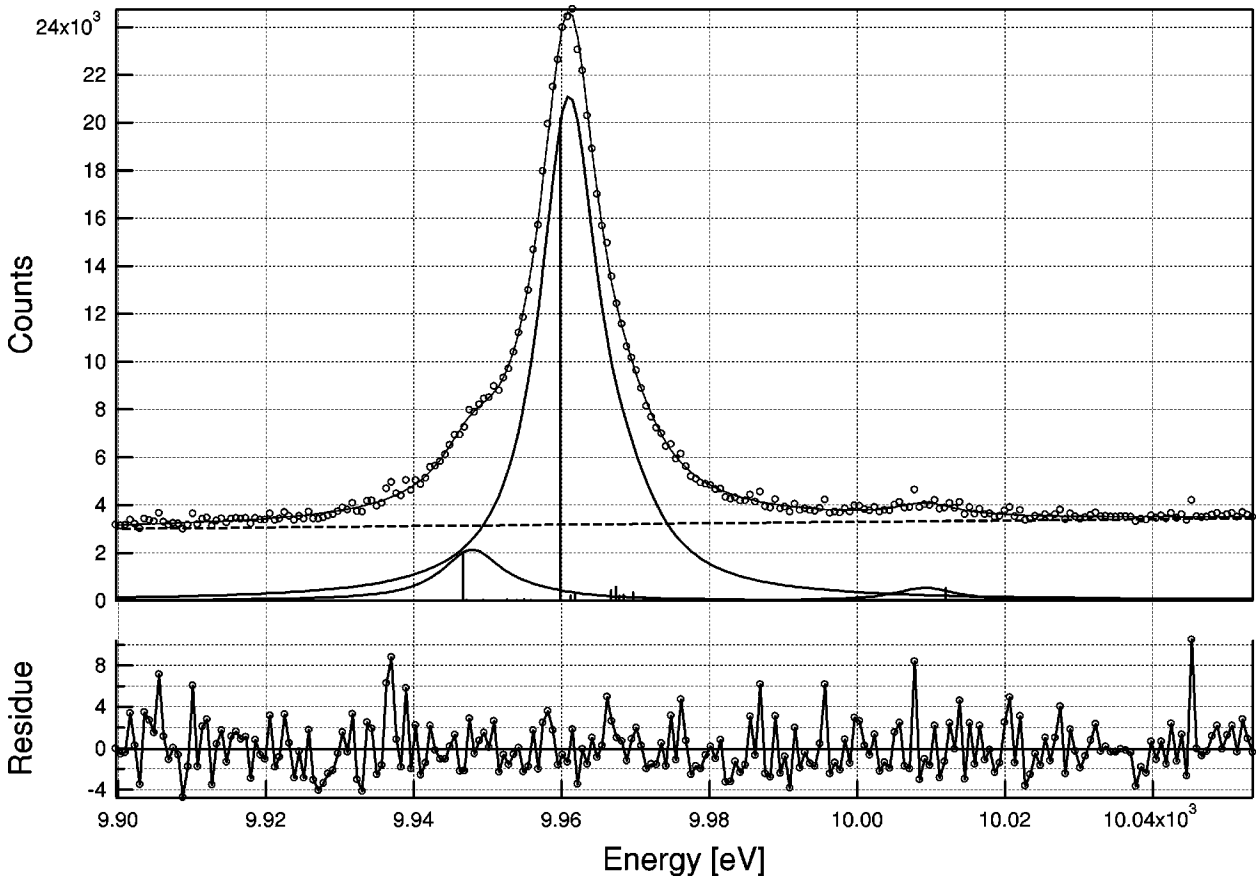


FIG. 2. W $L\beta_{2,15}$ emission spectra.

We used for $\omega_i$ the values reported by Krause [26], for $\sigma_i$ the values reported by Reusch [27] for $_{73}$Ta at 50 kV, and for $P(L_iL_jX)$ the values reported by Chen *et al.* [28]. The values of the relative intensities of the satellite lines originated from Coster-Kronig transitions for $L\alpha_{1,2}$ and $L\beta_{1,2}$ are presented in Table III together with their corresponding energy position. In this table, the Coster-Kronig channel for creating *M*-shell spectator holes is closed. The energy positions of the satellite lines are the results of *ab initio* relativistic calculations of *L*-series x-ray satellites that arise from the presence of one spectator hole in the *M* or *N* shells of the emitting atoms, published by Parente *et al.* [25].

From the energy position of the *N*-shell spectator-hole satellite transitions one can observe that these lines can be separated into two groups: the $N_1$-$N_5$ transitions, characterized by a higher-energy position compared with the diagram line and providing the main part of the satellite transitions ($>60\%$), and the $N_6$-$N_7$ transitions, having the lower energy, but very close to the diagram line. For the *O* and *P* shells we could not separate the relative energy position of spectator hole from the diagram line. The relative intensity of these satellites together is about 1.52% in the case of $L_2$ initial vacancy state transitions and about 0.86% in the case of $L_3$ initial vacancy state transitions.

Although there is an energy difference for the diagram lines between the theoretical values and the experimental values published by Bearden [11], in the multiplet fitting method only the relative position and the relative intensity of the satellite lines to the diagram line is important, which together give the line shape of the spectra. As a result of fitting one can obtain the linewidth of each group, considered as a diagram line and its satellites, the energy shift of the whole group, and the amplitude.

## IV. $L\beta_2$ VISIBLE SATELLITE

It was considered that the Coster-Kronig transition $L_1 \rightarrow L_3\ M_5$ is energetically forbidden according to the theoretical calculations of Chen *et al.* [10], because the energy difference between levels $L_1$ and $L_3\ M_5$ is $-2.70$ eV. However, recently, Salguero *et al.* [3] suggested that the Coster-Kronig channel might be actually open from their experimental results that the relative intensity $I_s$ of the $L\beta_2$ visible satellite to the diagram $L\beta_2$ line shows an increase with exciting energy below 20 keV and is almost constant above it.

The results of the dependence of $I_s$ on the exciting energy are shown in Fig. 3. The relative intensity of the satellite line with respect to the $L\beta_2$ line, $I_s(E)$, shows a slow increase as a function of exciting energy, which suggests a shake-off process rather than a Coster-Kronig transition. This fact was also confirmed by another experiment with different crystal. As described by Armen *et al.* [29], the dependence of the shake-up probability in the shake process on the exciting electron energy has a sharp finite onset and reaches the sudden limit quickly, while the shakeoff probability starts from zero at the threshold, increases slowly, and approaches the sudden limit gradually. However, the probability of a shake-off transition (for example, the total probability of the shake process is $2.4\times10^{-3}$ for $[2p3l]$) is much more smaller than the values obtained in our experiment.

TABLE III. W $L$ satellite lines due to $N$-, $O$-, and $P$-shell spectator holes: average energies and relative intensities.

| | $L_2$ transitions | | | $L_3$ transitions | | | | |
|---|---|---|---|---|---|---|---|---|
| Spectator hole $X_i$ | $L\beta_1$ group $L_2X_i$-$X_iM_4$ $E_{av}$ (eV) | $L\gamma_1$ group $L_2X_i$-$X_iN_4$ $E_{av}$ (eV) | $I_s$ [%] | $L\alpha_1$ group $L_3X_i$-$X_iM_5$ $E_{av}$ (eV) | $L\alpha_2$ group $L_3X_i$-$X_iM_4$ $E_{av}$ (eV) | $L\beta_2$ group $L_3X_i$-$X_iN_5$ $E_{av}$ (eV) | $L\beta_{15}$ group $L_3X_i$-$X_iN_4$ $E_{av}$ (eV) | $I_s$ [%] |
| Diagram Line | **9670.63** | **11281.4** | | **8398.47** | **8335.84** | **9959.83** | **9946.65** | |
| $M1$ | 9696.198 | 11 337.5 | 0 | 8419.095 | 8358.294 | 10 012.62 | 10 000.15 | 0 |
| $M2$ | 9693.727 | 11 333.6 | 0 | 8426.827 | 8370.728 | 10 022.51 | 10 008.47 | 0 |
| $M3$ | 9696.926 | 11 338.7 | 0 | 8418.913 | 8355.607 | 10 009.54 | 9998.214 | 0 |
| $M4$ | 9696.795 | 11 342.1 | 0 | 8425.891 | 8365.089 | 10 025.65 | 10 012.09 | 0 |
| $M5$ | 9696.347 | 11 344.8 | 0 | 8422.705 | 8356.652 | 10 017.75 | 10 005.36 | 0 |
| $M_1-M_5$ | | | **0.00** | | | | | **0.00** |
| $N1$ | 9674.198 | 11 291.5 | 0 | 8401.084 | 8338.768 | 9968.419 | 9955.869 | 1.17 |
| $N2$ | 9672.813 | 11 291.7 | 2.77 | 8402.408 | 8340.02 | 9969.665 | 9959.793 | 1.72 |
| $N3$ | 9674.555 | 11 290.0 | 2.82 | 8400.935 | 8338.597 | 9967.844 | 9954.016 | 1.04 |
| $N4$ | 9673.377 | 11 289.0 | 0.79 | 8401.428 | 8339.59 | 9967.304 | 9954.903 | 2.83 |
| $N5$ | 9673.473 | 11 288.3 | 1.06 | 8400.823 | 8337.777 | 9966.724 | 9952.579 | 2.17 |
| $N_1-N_5$ | **9673.627** | **11 290.28** | **7.44** | **8401.367** | **8339.01** | **9967.827** | **9955.303** | **8.93** |
| $N6$ | 9669.713 | 11 283.7 | 2.13 | 8397.161 | 8335.164 | 9961.193 | 9949.392 | 1.08 |
| $N7$ | 9669.12 | 11 282.1 | 2.80 | 8397.524 | 8334.227 | 9961.844 | 9947.123 | 1.37 |
| $N_6-N_7$ | **9669.376** | **11 282.79** | **4.93** | **8397.364** | **8334.64** | **9961.557** | **9948.123** | **2.45** |
| $O1$ | | | 0.56 | | | | | 0.22 |
| $O2$ | | | 0.37 | | | | | 0.26 |
| $O3$ | | | 0.37 | | | | | 0.16 |
| $O4$ | | | 0.06 | | | | | 0.20 |
| $P1$ | | | 0.16 | | | | | 0.02 |
| $O_1-P_1$ | | | **1.52** | | | | | **0.86** |
| Total | | | **13.92** | | | | | **12.27** |

## V. CONCLUSIONS

The reliable values of natural linewidth and relative intensities of the main $L$-emission lines of tungsten were obtained by means of the multiplet fitting with the satellite structure. For the disagreement between theory and experiment for $L_i \rightarrow N_j$ transitions, the theoretical reestimate with relativistic calculations is necessary. The relative intensity $I_s$ for the $L\beta_2$ visible satellite increases with increasing exciting energy and this tendency is similar to the threshold behavior of the shake-off process. However, its theoretical probability is too small to assign, compared with the values obtained in our experiment. As suggested by Salguero *et al.*, the strong dependence of the $L_{1,2,3}$-subshell ionization cross section on the exciting electron energy probably will have to be taken in account.

In the future, in order to elucidate the mechanism of the visible satellite of $L\beta_2$ for $_{74}$W, the x-ray emission spectra will be investigated as a function of incident photon energy with tunable synchrotron radiation sources. It is also interesting to perform such experiments for the neighboring elements $_{73}$Ta and $_{75}$Re.

## ACKNOWLEDGMENTS

We thank Y. Isozumi for his continuous support. We are also grateful to Katsumi Kondo, Shuichi Emura, and Kazuhiko Omote for their kind cooperation to this project. We appreciate K. Tanno for his helping to make the slits.

## APPENDIX: PROPERTIES OF THE VOIGT FUNCTION

As can be seen from Eq. (3), the value of the Voigt function at the origin ($E_0$) is equal to the amplitude ($A$): $V(0,y)=A$. When the dispersion tends to zero the Voigt function becomes a Lorentzian:

$$V(x\rightarrow\infty,y\rightarrow\infty)=\frac{A}{1+[2(E-E_0)/w]^2}. \tag{A1}$$

Similarly, when the width of the Lorentzian tends to zero, the Voigt function becomes a Gaussian with the width equal to the dispersion parameter:

$$V(x,y\rightarrow 0)=Ae^{-(2\sqrt{\ln 2}(E-E_0)/d)^2}. \tag{A2}$$

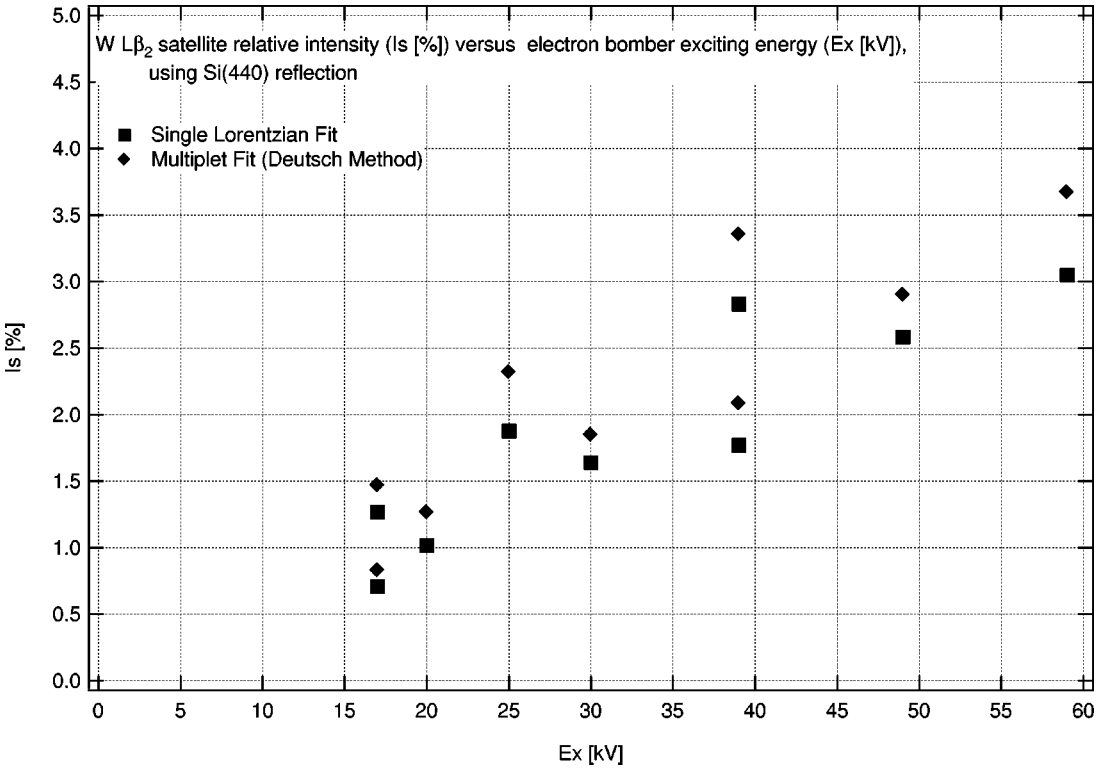


FIG. 3. Relative intensity $I_s$ of W $L\beta_2$ visible satellite as a function of exciting electron energy.

The Lorentzian width and the dispersion width both have full width at half maximum (FWHM). The width of the Voigt function itself can be approximated [16] as follows:

$$w_v = \frac{w}{2} + \sqrt{\left(\frac{w}{2}\right)^2 + d^2}. \tag{A3}$$

The area of the Voigt function given in Eq. (3) is

$$S_v = \frac{1}{2}\frac{Ad}{K(0,y)}\sqrt{\frac{\pi}{\ln 2}}, \tag{A4}$$

where $y(w,d)$ is the shape parameter given in Eq. (6).

Consider the convolution $g(x)$ of a function $f(x)$ with the weighting function $h(x)$:

$$g(x) = \int h(t) f(x-t)\,dt. \tag{A5}$$

Integrating in respect with $x$ and changing the order of integration we obtain

$$\begin{aligned}\int g(x)\,dx &= \int \left( \int h(t) f(x-t)\,dt \right) dx \\ &= \int h(t) \left( \int f(x-t)\,dx \right) dt \\ &= \int h(t)\,dt \int f(y)\,dy \end{aligned} \tag{A6}$$

after changing $x-t=y$, $dx=dy$. If the weighting function $h(x)$ is normalized, the area of the convoluted function $g(x)$ is equal to the area of the function $f(x)$. In the case of the Voigt function, the Gaussian plays the role of the normalized weighting function. Therefore, the area of the Voigt function is also equal to the area of the Lorentzian:

$$S_v = S_L = \frac{\pi}{2} A_L w. \tag{A7}$$

From Eq. (A4) we can immediately determine the amplitude of the Lorentzian, which convoluted with the normalized Gaussian weighting function gives the Voigt profile.

[1] A. N. Nigam and R. B. Mathur, Chem. Phys. Lett. **28**, 41 (1974).
[2] A. N. Nigam, R. B. Mathur, and R. Jain, J. Phys. B **7**, 2489 (1974).
[3] L. Salgueiro, M. L. Carvalho, and F. Parente, J. Phys. (Paris), Colloq. **48**, C9-609 (1987).
[4] S. I. Salem and P. L. Lee, Phys. Rev. A **10**, 2033 (1974).
[5] S. I. Salem, S. L. Panossian, and R. A. Krause, At. Data Nucl. Data Tables **14**, 91 (1974).
[6] B. G. Gokhale, S. N. Shukla, and Raman Nath Srivastava, Phys. Rev. A **28**, 858 (1983).
[7] E. J. McGuire, Phys. Rev. A **5**, 1043 (1972).
[8] E. J. McGuire, Phys. Rev. A **6**, 851 (1972).
[9] E. J. McGuire, Phys. Rev. A **10**, 13 (1974).

[10] M. H. Chen, B. Crasemann, K. N. Huang, M. Aoyagi, and H. Mark, At. Data Nucl. Data Tables **19**, 97 (1977).
[11] J. A. Bearden, Rev. Mod. Phys. **39**, 78 (1967).
[12] A. E. Sandström, *Experimental Methods of X-ray Spectroscopy, Ordinary Wavelengths*, edited by S. Flügge, Handbuch der Physik Vol. 30 (Springer-Verlag, Berlin, 1957), p. 78–245.
[13] F. Schreier, J. Quant. Spectrosc. Radiat. Transf. **48**, 743 (1992).
[14] J. Humlič ek, J. Quant. Spectrosc. Radiat. Transf. **27**, 437 (1982).
[15] S. R. Drayson, J. Quant. Spectrosc. Radiat. Transf. **16**, 611 (1975).
[16] E. E. Whiting, J. Quant. Spectrosc. Radiat. Transf. **8**, 1379 (1968).
[17] B. H. Armstrong, J. Quant. Spectrosc. Radiat. Transf. **7**, 61 (1968).
[18] M. S. Chen, B. Crasemann, and H. Mark, Phys. Rev. A **24**, 177 (1981).
[19] M. S. Chen, B. Crasemann, and H. Mark, Phys. Rev. A **27**, 2989 (1983).
[20] M. S. Chen, B. Crasemann, and H. Mark, Phys. Rev. A **21**, 449 (1980).
[21] E. J. McGuire, Phys. Rev. A **9**, 1840 (1974).
[22] M. O. Krause and J. H. Oliver, J. Phys. Chem. Ref. Data **8**, 329 (1979).
[23] M. Deutsch, G. Hölzer, J. Härtwig, J. Wolf, M. Fritsch, and E. Förster, Phys. Rev. A **51**, 283 (1995).
[24] J. H. Scofield, At. Data Nucl. Data Tables **14**, 121 (1974).
[25] F. Parente, M. H. Chen, and B. Crasemann, At. Data Nucl. Data Tables **26**, 383 (1981).
[26] M. O. Krause, J. Phys. Chem. Ref. Data **8**, 307 (1979).
[27] S. Reusch, H. Genz, W. Low, and A. Richter, Z. Phys. D **3**, 379 (1986).
[28] M. H. Chen, B. Crasemann, H. Mark, M. Aoyagi, and H. Mark, At. Data Nucl. Data Tables **24**, 13 (1979).
[29] G. B. Armen, T. Åberg, Kh. R. Karim, J. C. Levin, B. Crasemann, G. S. Brown, M. H. Chen, and G. E. Ice, Phys. Rev. Lett. **54**, 182 (1985).